Investigation on a New Approach for Designing Articulated Soft Robots With Discrete Variable Stiffness

Yong Zhong, *Member, IEEE*, Ruxu Du, Peng Guo, and Haoyong Yu, *Member, IEEE*

***Abstract*—Soft robots made of elastic and compliant materials offer various advantages, such as safe interaction, adaptiveness, and easy fabrication. However, the highly dissipative nature of elastic materials intrinsically limits certain functions, such as force transmission, positioning accuracy, and load capability. Herein, in this article, we present a design approach for developing articulated soft robots with variable stiffness. We propose a bioinspired bistable articulated joint that consists of a rigid joint and bistable structures. We realize stiffness change through forming a locking function by triggering the bistable structure to switch between two stable states. The trigger force is generated by heating shape memory alloy springs connected to the bistable structures. After the locking function is triggered, the bending stiffness of the articulated joint is highly amplified. Moreover, the joint can be locked at different angles through mechanically preprograming bistable structures fabricated with a single three-dimensional print. With this approach, we developed an articulated soft robot as a case study. The robot demonstrated variable stiffness, changeable configurations, and a large workspace. Moreover, the approach proposed in this article provides valuable insights into the utilization of bistability for developing variable-stiffness robotic systems.**

***Index Terms*—Articulated soft robot, bistable structure, locking function (LF), variable stiffness.**

Manuscript received May 14, 2020; revised August 28, 2020 and November 24, 2020; accepted December 30, 2020. Date of publication January 6, 2021; date of current version December 15, 2021. Recommended by Technical Editor H. Wang Alanis and Senior Editor G. Alici. This work was supported in part by the Strategic Priority Research Program of the Chinese Academy of Sciences (Class A) under Grant XDA22040203, in part by the Fundamental Research Funds for the Central Universities under Grant 2019XX01, in part by GDNRC [2020] 031, and in part by the Natural Science Foundation of Guangdong Province under Grant 2020A1515010621. *(Corresponding author: Haoyong Yu.)*

Yong Zhong and Ruxu Du are with the School of Intelligent Engineering, South China University of Technology, Guangzhou 511442, China (e-mail: zhongyong@scut.edu.cn; duruxu@scut.edu.cn).

Peng Guo is with the Changchun Institute of Optics, Fine Mechanics and Physics, Chinese Academy of Sciences, Changchun 130033, China (e-mail: guopenghust@hotmail.com).

Haoyong Yu is with the Department of Biomedical Engineering, National University of Singapore, Singapore 119077, Singapore (e-mail: bieyhy@nus.edu.sg).

Color versions of one or more figures in this article are available at https://doi.org/10.1109/TMECH.2021.3049592.

Digital Object Identifier 10.1109/TMECH.2021.3049592

I. Introduction

SOFT robots are normally constructed of elastic materials and compliant structures, and they have several unique advantages, such as simple structure, safe interaction, adaptiveness, easy actuation, and easy fabrication [1]. However, soft robotic systems, which mimic invertebrates with soft bodies, have low precision, poor repeatability, small load capability, and low stiffness when completing most industrial tasks, which limits their extensive application. Unlike invertebrates, most other animals consist of rigid structures with soft tissue, such as muscle, fat, and skin. The rigid structures are responsible for most of the weight support and force transmission, and they are essential for locomotion and maneuvering. Moreover, variable stiffness for a soft robot can enable its adaption to different requirements, such as bearing different loads and changing manipulation stiffness. Thus, many scientists and engineers have been working on improving the stiffness of soft robots. The existing approaches to solving this problem can be divided into two categories: material stiffening methods and mechanical stiffening methods.

The material stiffening methods involve changing Young's modulus of material or facilitating material deformation through the use of external stimulus. Shape memory materials have been employed to realize stiffness change of bioinspired robots, such as utilizing shape memory alloys and shape memory polymers to alter the flexural stiffness of soft robots and the stiffness of beam [2], [3]. Dielectric elastomers, another type of material suitable for electrically activated soft robots, have been exploited to vary the stiffness of soft robots [4] by varying the applied voltage alone. Low-melting-point materials and glass transition-based softening have also been integrated into soft robots to vary their stiffness [5], [6]. Cheng *et al.* [7] presented an approach that involved coating wax on flexible open cells to realize a broad range of stiffness changes and applied it to locking joint systems and shape-shifting structures. To achieve higher levels of stiffness variation, low-melting-point alloys need to be used in soft robots [8]. Another approach is the use of magneto- and electrorheological materials, the rheological properties of which can be changed by applying a magnetic or electric field. In summary, material stiffening methods can be used to vary the stiffness of soft robots but they suffer from a few shortcomings, such as encapsulation difficulty, integration, fabrication, and energy inefficiency. Moreover, they cannot be

changed to be large stiffness, which limits their use in real applications.

Mechanical stiffening methods have been employed to realize variable stiffness in soft robots. For example, soft pneumatic actuators with antagonistic actuation can be used to increase the stiffness of actuators by applying opposing forces [9]–[11]. Fluid-driven robotic systems with origami structures have been designed to achieve large load capability, and flexible arms comprising vacuum-driven joints have achieved reliable stiffness [12], [13]. Jamming technology was utilized to build soft robots and there exist two systematic approaches that exploit the jamming phenomenon: membranes filled with the granular matter or with thin sheets. The actuation principle is that vacuum can increase the relative shear stress experienced by the particles or layers in the elastic; then, the stiffness of the medium can be changed to modulate the robots' direction and magnitude during operation [14]–[17]. All of these approaches require a continuous supply of energy, and the resulting robots are prone to problems associated with sealing and leakage. Purely mechanical mechanisms can be used to realize variable stiffness in soft robots. For example, Degani *et al.* [18] developed a snake robot for minimally invasive surgery. This robot consists of an inner snake robot and an outer snake robot that mechanically constrain each other. These mechanical constraints change the stiffness of the articulated soft robot. Similar approaches have been proposed, such as those by Li *et al.* [19] and Yuyu *et al.* [20], who used telescopic tubes or spines to constrain the flexibility of a soft robot, leading to a change in stiffness. Although the approaches based on mechanical mechanisms have some limitations, such as mechanical complexity, weight, and size, the resulting robots have considerable stiffness owing to the aforementioned mechanical constraints, and they can be easily implemented in real applications.

In this article, we developed a new approach to achieve variable stiffness in soft robots. We invented a bioinspired bistable articulated joint (BBAJ) that employs bistable actuation to achieve stiffness change. Bistable actuation can be observed in biological systems, such as the Venus flytrap [21] and the Mantis shrimp [22], which rely on this type of actuation to prey and defend. A bistable structure has three mechanical states: two stable states and one instable state, and the switch between the two stable states only needs a small trigger force at the instable transition position [23]. This is an effective method for maintaining the states of a robotic system without a continuous power supply, and it can act as an amplifying mechanism to transmit displacement and force [24]. Engineers found a lot of interests in incorporating bistabilities into the designs of mechanical systems, such as flytrap-inspired robots [25], [26], microbistable devices [27], morphing and energy harvesting mechanisms [28]–[30], and injection molding [31], [32]. Unlike the aforementioned usage of bistabilities, we utilize a bistable structure to achieve stiffness change for articulated soft robots. Moreover, we apply electric current to SMA springs to trigger the bistable structures of the BBAJ, and the snap instability of the bistable structure can instantaneously generate large geometrical changes. Then, the BBAJ is mechanically locked, which results in a massive increase in the bending stiffness of the structure.

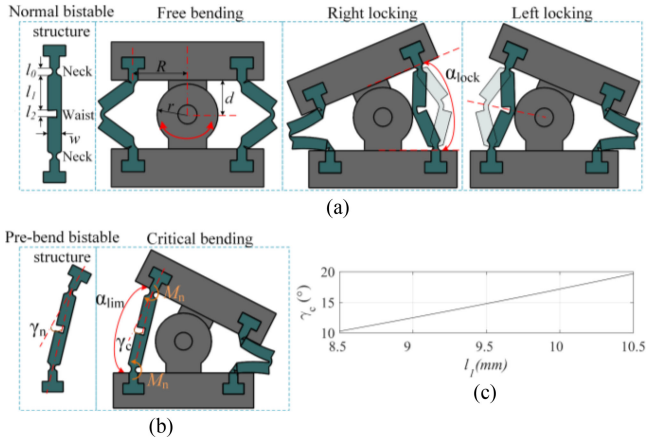

Fig. 1. Design concept of the BBAJ. (a) Schematic of the normal bistable structure, and the three states of the conceptually designed BBAJ. (b) Schematic of the prebend bistable structure with a bending angle of γ_n of the neck, limit bending state of the BBAJ. (c) Relationship between the critical neck bending angle γ_c and beam length (l_1).

Owing to this unique design and implementation of the bistable structure and the SMA trigger approach, the BBAJ is capable of stiffness change. Accordingly, we constructed an articulated soft robot using BBAJs to demonstrate our approach. In the articulated soft robot, each joint is connected by bistable structures triggered by SMA springs, and once the robot bends to the target angle, the joint can be selectively locked to maintain its bending angle, resulting in numerous robot configurations with fewer actuators and the achievement of a variable workspace. With these characteristics, through appropriate design, we can envision the development of diverse applications, ranging from industrial soft robot arms to biological soft robots.

II. Materials and Methods

In this section, we present the design and modeling of the BBAJ and expound the principles of bistable actuation.

A. BBAJ Design

Bistable actuation is commonly found in biological systems. Herein, we integrate bistable actuation in an articulated joint to achieve stiffness change through a locking function (LF).

Fig. 1 shows a conceptual design of the BBAJ to illustrate the actuation principles of bistable structures in an articulated joint. The bistable structure is designed to be similar to a flexible hinge, where the neck and waist parts can be deformed easily [the first picture in Fig. 1(a)] and is installed on both sides of a pin joint. The BBAJ exhibits three states: free bending, right locking, and left locking, in which the right and left locking are achieved by triggering the bistable structure on the locking side to transition from outward deformation to inward deformation; at this point, the inward deformation causes physical contact between the waist and the rigid pin joint, obtaining the locking angle α_{lock} [i.e., physical locking, the third picture in Fig. 1(a)]. This physical locking state can magnify the bending stiffness of the joint in the corresponding locking direction. Once the joint is in the locking state, it does not need external energy to maintain

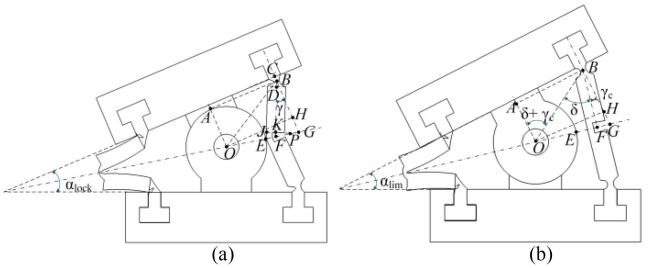

Fig. 2. Geometrical schematic of BBAJ. (a) Locking state. (b) Limit bending state.

the state. The primary design metrics of the BBAJ are locking angle α_{lock} and limit bending angle α_{lim} (see Fig. 2), the latter obtained when the waist angle is zero

The locking angle α_{lock} is determined by the dimensional parameters of both the joint and the bistable structure [see Fig. 2(a)]. To enable the BBAJ modular to adapt different designs of bistable structures, the dimensions of the joint are set to be constant. Thus, the parameters of the bistable structure are used to mechanically program the locking angle based on the relationship between deformation and geometry. The main parameters of the bistable structure are neck length l_0, beam length l_1, beamwidth w, and waist length l_2. Given that the thickness of the bistable structure does not affect the geometric relationship of the joint, we do not address it here. The locking angle can be calculated at the critical situation that the bistable structure just comes into physical contact with and is supported by the pin joint at point E [see Fig. 2(a)]. Because the bending angle of the neck γ of the bistable structure is relatively small, it can be considered a flexible hinge, and we assume the beam has no deformation; thus, BC = BD $\approx l_0/2$. The other parameters can be expressed as follows: d is half of the joint gap, BH = AO = d - $l_0/2$, OE = r, OH = AB = R, JE = $l_2/2$, JK = w/2, $\angle$FBG = γ, $\angle$HOG = $\frac{\alpha_{lock}}{2}$, and set OH$\perp$BG. Thus, in ΔEPJ, based on complement angle relationship, we have $\angle$JEF = $\frac{\alpha_{lock}}{2} + \frac{\pi}{2} - \gamma$. Then, in ΔBFG, based on the Law of Sines, we have

$$\frac{\text{BG}}{\sin\left(\frac{\alpha_{\text{lock}}}{2}+\frac{\pi}{2}-\gamma\right)} = \frac{\text{BF}}{\sin\left(\frac{\pi}{2}-\frac{\alpha_{\text{lock}}}{2}\right)} = \frac{\text{FG}}{\sin\gamma} \tag{1}$$

in which

$$\text{BG} = \text{HG}+\text{BH} = \text{R}\tan\frac{\alpha_{\text{lock}}}{2} + \left(d-\frac{l_0}{2}\right) \tag{2}$$

$$\text{BF} = \text{BK}+\text{KF} = \left(\frac{l_0}{2}+l_1\right) + \left(\frac{l_2}{2}-\frac{w}{2}\cot\left(\frac{\alpha_{\text{lock}}}{2}+\frac{\pi}{2}-\gamma\right)\right) \tag{3}$$

$$\text{FG} = \text{OG}-\text{OE}-\text{EF} = \frac{R}{\cos\frac{\alpha_{\text{lock}}}{2}} - r - \frac{w}{2\sin\left(\frac{\alpha_{\text{lock}}}{2}+\frac{\pi}{2}-\gamma\right)}. \tag{4}$$

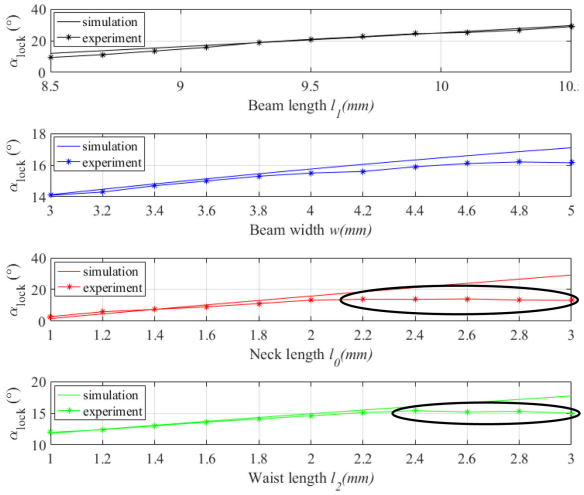

Fig. 3. Predictions and experimental results of the locking angle with respect to beam length, beamwidth, neck length, and waist length. All of the bistable structures with different parameters were directly 3-D printed. The reference geometry for the parameters is: l_0 = 2 mm, l_1 = 9.5 mm, l_2 = 2 mm, w = 3.6 mm, R = 14.75 mm, d = 9 mm, and r = 8.5 mm.

Based on (1)–(4), we can obtain the bending angle of the neck γ and the locking angle α_{lock}. However, due to the complexity of the functions, the explicit solutions cannot be obtained, we can still get the numerical results.

All parameters of the bistable structure affect the locking angle. We simulated the relationships between locking angle and these parameters, fabricated bistable structures through three-dimensional (3-D) printing, and measured the locking angles one by one. For a fair comparison, the length ranges of the parameters were within 2 mm. The simulation results (see Fig. 3) indicated that the beam length was the most influential parameter, followed by the neck length, waist length, and beamwidth. However, the experimental results indicated that the corresponding locking angles for neck length and waist length had large relative errors compared with the predictions. This could be attributed to the fact that when the lengths of the neck and waist became too long, the deformations of them were not standard beam-bending deformation any more due to the constraints and reactive forces from the joint, and the material using in experiments is TPU95 which is flexible, thus the deformations for all the parameters exist. We can further check this fact in the last two pictures of Fig. 3, where the experimental results of locking angles decrease with the increase of the neck length and waist length, which indicate unexpected deformations happened (tagged by a black ellipse). Thus, to design an appropriate bistable structure for BBAJ, the lengths of the neck and waist should be small enough to make sure the linear variation for locking angle.

The limit bending angle α_{lim} is determined at the position at which the bistable structure is pulled to its largest length within the applied geometric constraints. The critical bending angle γ_{c} of the neck is depicted in Fig. 2(b) ($\angle$FBG = γ_{c}). Here, AO = d - $l_0/2$, OE = r, GB$\perp$BA, and BF $\approx l_0/2 + l_1 + l_2/2$. At this position, the waist of the bistable structure is straight, that is,

BF⊥OG. Thus, the relationship can be expressed as follows:

$$\sin\delta = \frac{\mathrm{OF}}{\mathrm{OB}} = \frac{\sqrt{(\mathrm{AB}^2+\mathrm{AO}^2)-\mathrm{BF}^2}}{\mathrm{OB}} = \frac{\sqrt{R^2+(d-l_0/2)^2-(l_0/2+l_1+l_2/2)^2}}{\sqrt{R^2+(d-l_0/2)^2}} \tag{5}$$

$$\sin(\delta+\gamma_c) = \frac{\mathrm{AB}}{\mathrm{OB}} = \frac{R}{\sqrt{R^2+(d-l_0/2)^2}} \tag{6}$$

$$\gamma_c = \sin^{-1}\frac{R}{\sqrt{R^2+(d-l_0/2)^2}} - \delta. \tag{7}$$

At this critical position, the limit bending angle is then given by

$$\alpha_{lim} = 2\gamma_c. \tag{8}$$

B. Spontaneous Recovery Characteristics

When the BBAJ needs to recover from the locking state to the free-bending state, one would generally be more likely to apply a pulling force to deform the bistable structure outward. However, we adopt a different approach and utilize the potential energy generated by the deformation of the bistable structure to help it recover to the free-bending state. The normal bistable structure is designed to be straight [see Fig. 1(a)]; thus, the potential energy always tends to recover the deformed structure to be straight. When the joint continues to bend opposite to the locking direction and reaches the limit bending angle α_{lim}, the bending angle of the waist is zero, and the potential energy of the deformed necks generates moments M_n that tend to bend the bistable structure outward [see Fig. 1(b)]. Thus, we simply need to bend the joint to the limit bending position and release it, which causes the bistable structure to deform outward and, consequently, the BBAJ to recover to the free-bending state. The bending angle of the neck at this critical position γ_{c} can be treated as the reference angle of the neck for designing the spontaneous recovery characteristic of BBAJ, and it has an approximately linear relationship with the beam length l_1 based on (7) [also shown in Fig. 1(c)]. As shown in Fig. 1(b), when a prebend bistable structure is used to replace the normal one, the designed bending angle of the neck γ_{n} can determine the magnitude of the moment when the joint bends to the limit bending angle. The trick is that if $\gamma_{\mathrm{n}} < \gamma_{\mathrm{c}}$, the bistable structure can spontaneously recover to the free-bending state; otherwise, it requires additional actuation to pull the structure to deform outward. The spontaneous recovery characteristic can also be achieved by prebending the waist of the structure. In both, the aforementioned approaches, the pre-bend moment of the structure is used for recovery. In this article, we use the prebend neck structure as an example.

C. Bistable Actuation Principles

To trigger the BBAJ to transition from the free-bending state to the locking state, the trigger force must overcome the energy barrier of the compliant bistable structure. To study the bistable actuation principles and find the qualitative force trend, we qualitatively analyze the bistable actuation of the bistable structure in the BBAJ, and we make the following assumptions:

1) the thicknesses of the necks and waist are considerably smaller than that of the beams, and the deformation of the beam is ignored in the model;
2) when torque is applied to the bistable structure, the beams can be regarded as truss bars with no compression and flection;
3) during analysis, the physical constraint that the structure touches the joint pin is not expressed in the model;
4) the initial bending angle α of the BBAJ is motor controlled through cables and the variation is quite small during the bistable actuation process, thus we use axial displacement (ΔL) of the bistable structure to approximate the effect of a small variation of joint initial bending angle α. We now consider half of the structure because of its symmetric geometry and model the bending motions of the neck and waist as pin joints with torsional springs (see Fig. 4).

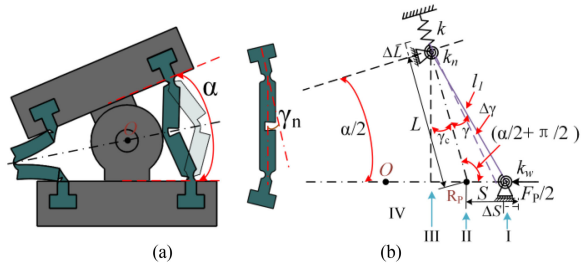

Fig. 4. Idealization of the truss model of the BBAJ. (a) Three-dimensional model of the BBAJ and the bistable structure. (b) Idealization of the truss model for bistable actuation analysis.

We use Lagrangian mechanics to construct the relationship between the required actuation force F_P and the distance S with respect to the reference point R_p (where the bending angle $\gamma = 0$) and the relationship between the potential energy and distance S. The Lagrangian function is expressed as

$$\mathcal{L} = T - \left(\frac{1}{2}k\Delta L^2 + \frac{1}{2}k_n(\gamma+\gamma_n-\Delta\gamma)^2 + \frac{1}{4}k_w(\alpha+2\gamma-2\Delta\gamma)^2\right), \tag{9}$$

where T is kinetic energy, k is the spring stiffness of axial displacement variation, k_n is the torsional spring stiffness of the neck, and k_w is the torsional spring stiffness of the waist. Then, Lagrange's equation is

$$\frac{\partial}{\partial \mathrm{t}}\left(\frac{\partial\mathcal{L}}{\partial\dot{q}}\right) - \frac{\partial\mathcal{L}}{\partial q} = Q. \tag{10}$$

Given that $T = 0$ (because the process is quasi-static), $q = \Delta S$, and the external force is $F_P/2$ can be expressed as

$$\frac{\partial\left(\frac{1}{2}k\Delta L^2 + \frac{1}{2}k_n(\gamma+\gamma_n-\Delta\gamma)^2 + \frac{1}{4}k_w(\alpha+2\gamma-2\Delta\gamma)^2\right)}{\partial\Delta S} = \frac{F_P}{2}. \tag{11}$$

The relationship between ΔL and ΔS can be obtained by formulating a triangle with a constant beam length l_1 through Cosine Law

$$\cos\left(\frac{\alpha}{2}+\frac{\pi}{2}\right) = \frac{L^2+S^2-l_1^2}{2LS} = \frac{(L+\Delta L)^2+(S-\Delta S)^2-l_1^2}{2\,(L+\Delta L)\,(S-\Delta S)} \tag{12}$$

where $\boldsymbol{L}$ is the initial length between the neck spring and the reference point R_p. We rewrite the following equation as a function of ΔL:

$$\Delta L^2+2\Delta L\left(\Delta S\sin\frac{\alpha}{2}+L+S\sin\frac{\alpha}{2}\right)+\Delta S^2 - 2S\Delta S-2\Delta SL\,\sin\frac{\alpha}{2}=0 \tag{13}$$

and adopt the positive root

The neck angle variation $\Delta\gamma$ is expressed as follows:

$$\Delta\gamma = \sin^{-1}\frac{(S-\Delta S)\cos\frac{\alpha}{2}}{l_1} - \sin^{-1}\frac{S\cos\frac{\alpha}{2}}{l_1} \tag{15}$$

where the initial value of S is determined according to the parameters of the BBAJ and can be solved using

$$\cos\left(\frac{\alpha}{2}+\frac{\pi}{2}\right)=\frac{L^2+S^2-l_1^2}{2LS} \tag{16}$$

and adopting the positive root

$$S=\sqrt{l_1^2-\frac{L^2\,(1+\cos\alpha)}{2}}-L\sin\frac{\alpha}{2}. \tag{17}$$

Thus, through the combination of (12), (15), (16), and (18), the relationship between the applied force F_P and the distance ΔS can be obtained. To simplify the presentation, we write

$$F_P = kA-k_wB-k_nC \tag{18}$$

where unnumbered equation shown at the bottom of this page.

The potential energy induced by the deformation of the bistable structure itself is expressed as

$$P_s=\frac{1}{2}k_n(\gamma+\gamma_n-\Delta\gamma)^2+\frac{1}{4}k_w(\alpha+2\gamma-2\Delta\gamma)^2. \tag{19}$$

Based on (16), the potential energy can be rewritten as

$$P_s=\frac{k_w\left(\alpha+2\sin^{-1}\frac{(S-\Delta S)\cos\frac{\alpha}{2}}{l_1}\right)^2}{4} + \frac{k_n\left(\gamma_n+\sin^{-1}\frac{(S-\Delta S)\cos\frac{\alpha}{2}}{l_1}\right)^2}{2}. \tag{20}$$

Using this model, we can reveal and qualitatively analyze the principles governing the required actuation force and potential energy for the bistable actuation. Herein, examples of the bistable actuation process are illustrated in Fig. 5. In state I, no applied force is needed, and the joint is at the initial bending angle. Between states I and II, the bistable structure bends from the initial point to the reference point (distance $= 0$), where the neck angle is zero and the potential energy is approximately the minimum (valley), and the bistable force varies parabolically. Between states II and III, the bistable structure bends from the reference point R_p to close to the limit bending position (i.e., the waist is straight). Between states III and IV, the bistable structure executes a symmetric motion, as it does between states I and II. Notably, when $\alpha = 0°$, state II and state III refer to the same position. The two equilibrium states are approximately energetic (i.e., $|F_{P,\max}| \approx |F_{P,\min}|$), but they are affected by the uniform distribution of materials. The required trigger force applied on the waist of the bistable structure is approximately symmetrical with respect to the limit bending position (stage III). Notably, there are a few differences between the scenarios in which the prebend neck angle changes from 0° to 5° [see Fig. 5(a)]. The potential energy valley would be closer to the limit bending position, but the required force just moves a little to the negative direction of the

$$\Delta L=\sqrt{(S+\Delta S)^2\sin^2\frac{\alpha}{2}+2\,(LS+2L\Delta S)\sin\frac{\alpha}{2}+L^2+2S\Delta S-\Delta S^2}-L-(S+\Delta S)\sin\frac{\alpha}{2}. \tag{14}$$

$$A=2\left(\sin\frac{\alpha}{2}-\frac{S-\Delta S+S\sin^2\frac{\alpha}{2}+\Delta S\sin^2\frac{\alpha}{2}+2L\sin\frac{\alpha}{2}}{\sqrt{\left(L+S\sin\frac{\alpha}{2}\right)^2+(2S\Delta S+\Delta S^2)\sin^2\frac{\alpha}{2}+2S\Delta S-\Delta S^2+4L\Delta S\sin\frac{\alpha}{2}}}\right) \times\left(L+S\sin\frac{\alpha}{2}+\Delta S\sin\frac{\alpha}{2}-\sqrt{(S+\Delta S)^2\sin^2\frac{\alpha}{2}+2S\Delta S+L^2-\Delta S^2+2LS\sin\frac{\alpha}{2}+4L\Delta S\sin\frac{\alpha}{2}}\right)$$

$$B=\frac{2\cos\frac{\alpha}{2}\left(\alpha+2\sin^{-1}\frac{(S-\Delta S)\cos\frac{\alpha}{2}}{l_1}\right)}{l_1\sqrt{1-\frac{(S-\Delta S)^2\cos^2\frac{\alpha}{2}}{l_1^2}}}$$

$$C=\frac{2\cos\frac{\alpha}{2}\left(\gamma_n+\sin^{-1}\frac{(S-\Delta S)\cos\frac{\alpha}{2}}{l_1}\right)}{l_1\sqrt{1-\frac{(S-\Delta S)^2\cos^2\frac{\alpha}{2}}{l_1^2}}}$$

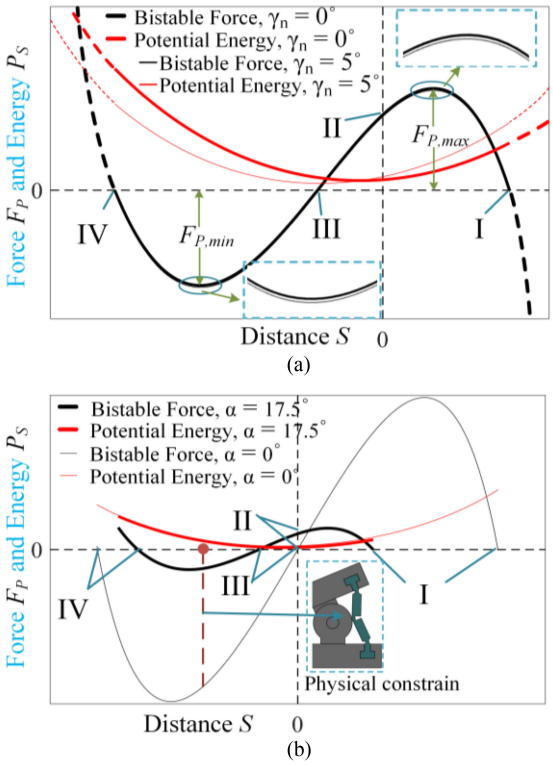

Fig. 5. (a) Principles of variation of the bistable actuation force (trigger force) and potential energy for different neck angles ($\gamma_n = 0°$ and 5°) when the initial bending angle is 17.5°. (b) Principles of variation of the bistable actuation force and potential energy for different initial bending angles ($\alpha = 0°$ and 17.5°) when the neck angle is 0°. The abscissa axis denotes the distance S.

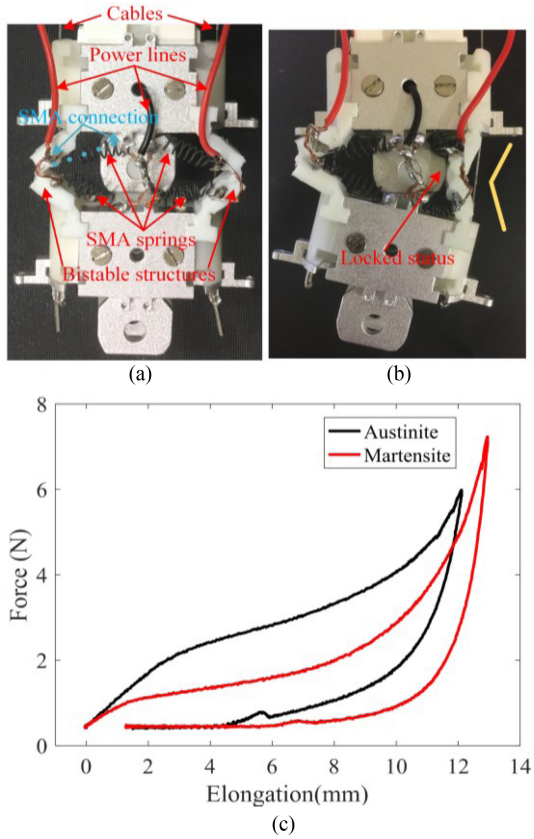

Fig. 6. (a) Deployment of the BBAJ. In the BBAJ, each bistable structure is connected to a pair of SMA springs between the beam and the metal shell of the joint. (b) Locking state of the BBAJ. The yellow polylines indicate the locking direction. (c) Typical force–displacement characteristics of the SMA spring.

Y-axis (i.e., $|F_{P,\max}| < |F_{P,\min}|$). Moreover, when the initial bending angle α of the joint decreases to zero (i.e., the links of the joint are parallel), the reference point coincides with the limit bending position and the required trigger force drastically increases [see Fig. 5(b)]. In the BBAJ, the bistable structure is constrained by the pin joint when bending inward (physical constraint indicated in Fig. 5(b)); at this moment, the trigger force decreases to zero, and the bistable structure cannot reach the theoretical position State IV. Because the beam is assumed to be axially rigid, the vertical deformation corresponding to the spring stiffness k has a few orders of magnitude larger than the corresponding torsional spring stiffness k_n, k_w of the bending of the bistable structure; and the changes of B and C terms in (19) influence a little on the force applied to the structure. Thus, the prebend neck angle γ_n in C terms has a negligible impact on the applied force, as indicated in Fig. 5(a). However, the potential energy induced by the deformation of the bistable structure itself changes with respect to the prebend angle. These principles of the bistable actuation offer guidance for the development of robots with bistable structures.

III. Deployment and Experiments

In this section, we describe the prototype of the BBAJ and, subsequently, present the experiments on bistable actuation force and displacement variations of the BBAJ. Thereafter, we conduct a finite-element analysis (FEA) for comparison.

A. BBAJ Integration

In the deployment of the BBAJ, dozens of methods can be used to supply the trigger force to the bistable structure, such as the use of a micromotor, cable-driven mechanism, and shape memory polymer and alloy. We use a type of SMA spring with a transition temperature of 45 °C (Kellogg's Research Labs) to trigger the structure because of its favorable characteristics, such as good repeatability, large force production, easy control, and compactness. Because the tensile force acting on the waist of the bistable structure may affect the strength of the thin waist and impede its outward bending, we connected the SMA springs to the beams of the bistable structure [see Fig. 6(a)]. Additionally, we connected them to a dc power supply operating under 5 V and actuated the joint through a pair of cables by using a servomotor. The locking process can be described as follows. First, the joint is driven to bend to the desired locking angle (normally close to the limit bending angle), and the SMA springs are activated to pull the bistable structure to bend inward with respect to the joint. Next, the servomotor is retracted to the locking angle to generate physical contact between the bistable structure and the rigid

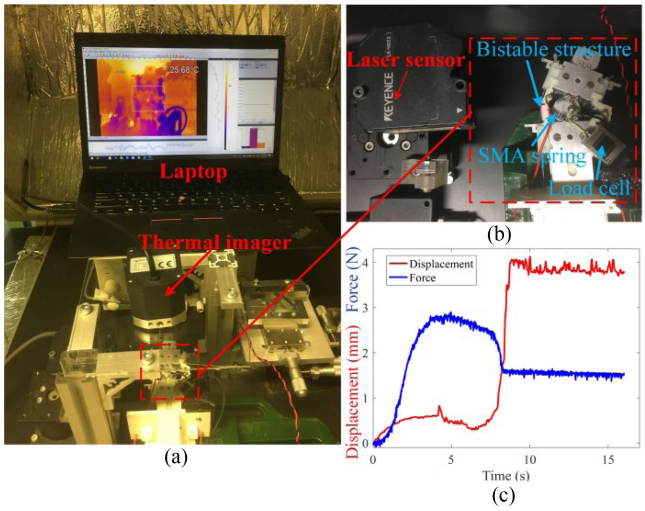

Fig. 7. Experimental setup for the BBAJ. (a) Setup used for real-time thermal imaging of the BBAJ actuation process, including the laptop, thermal imager, and the BBAJ. (b) Setup for measuring the actuation force and displacement of the bistable structure, including the laser sensor, SMA spring, and a load cell. (c) Variations in the tensile force of a single SMA spring and displacement of the bistable structure during the actuation process at the initial bending angle of 17.5°.

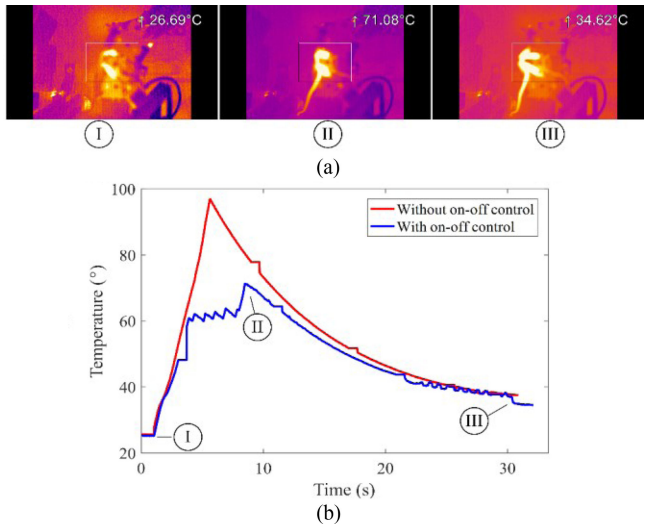

Fig. 8. BBAJ actuation process. (a) Thermal view of the actuation process. State Ⓘ marks the beginning of the actuation process, state Ⓘ represents the snap-through moment of the bistable actuation, and state Ⓘ marks the end of the cooling process. (b) Temperature variations with and without ON–OFF control.

inward part, and a stable double-triangular structure is obtained. Finally, the joint is locked in the inward direction [see Fig. 6(b)]. Based on the spontaneous recovery characteristic, the joint can recover to the free-bending state by being driven to bend to the limit bending position again. The force characteristics of the SMA springs adopted in this article are presented in Fig. 6(c).

The experimental setup used for testing the displacement and actuation force during the actuation of the bistable structure is presented in Fig. 7. A thermal imager (Optris PI) was set on top of the BBAJ to monitor the temperature variation of the SMA springs [see Fig. 7(a)]. One of the SMA springs was connected to a load cell (BangBu Sensor System Engineering, Co., Ltd.) to measure the actuation force, and a laser sensor (Keyence, Co., Ltd.) was installed to measure the displacement variation during actuation [see Fig. 7(b)].

The force variation characteristics of the SMA spring [see Fig. 6(c)] indicate that it can generate sufficient force to trigger the bistable structure. The variations of displacement and force indicate that when the bistable structure is pulled to the critical position [state II in Fig. 5(b)], both the force and displacement snap-through occur [see Fig. 7(c)]. The complete locking process of the BBAJ is achieved within 8 s. When the joint is locked in a very short time, the tensile force of the SMA spring suddenly decreases from 2.9 to 1.6 N and gently decreases thereafter as the temperature decreases, and the displacement increases to a constant value. The temperature of the SMA springs significantly affects the bistable actuation process. Therefore, we used the thermal imager to visualize the temperature variation and offer feedback to the controller. The controller can then control the ON–OFF states of the SMA springs by not only supplying the appropriate temperature to generate a sufficient actuation force for the bistable structure but also preventing overheating and consequential burning of the SMA springs. The thermal visualization and ON–OFF control of the SMA springs are illustrated in Fig. 8. In state Ⓘ, the SMA spring is activated and the temperature quickly increases. Without ON–OFF control, the temperature quickly increases to nearly 100 °C until the bistable structure is actuated to snap-through to the locking state (state Ⓘ); this high temperature may burn the SMA springs, which may cause them to lose their shape memory effect. With ON–OFF control, we can enable the appropriate actuation temperature for the bistable structure to be set and prevents burning of the SMA springs. The next actuation cycle can be executed only after the spring temperature decreases to the transition temperature of the SMA. The cooling process took approximately 20 s at room temperature (26 °C) in our experiment (state Ⓘ).

B. FEA of Bistable Actuation

The bistable actuation process was simulated on Ansys workbench. The upper joint link was treated as a rigid body, and the lower joint link was fixed during the simulation. Thus, we could treat the bistable structures as being fixed at the bottom. During the simulation, an appropriate force was first applied to the joint to move the joint to the real joint gap. The joint was then rotated to the initial bending angle. Finally, the joint was fixed at the initial bending angle, and a force was applied on the waist to initiate bistable actuation (Fig. 9(a), state Ⓘ). The bistable actuation process includes the transition from one equilibrium state to another, and it is a postbuckling process with relatively large deformation. The geometric nonlinearity caused by the large deformation must be considered in the simulation. Traditional nonlinear buckling analysis of the postbuckling of structures is usually ineffective for arriving at convergent solutions; thus, restart analysis is required to solve the convergence problem.

We conducted FEA with different initial bending angles to compute the critical trigger force required to just overcome the

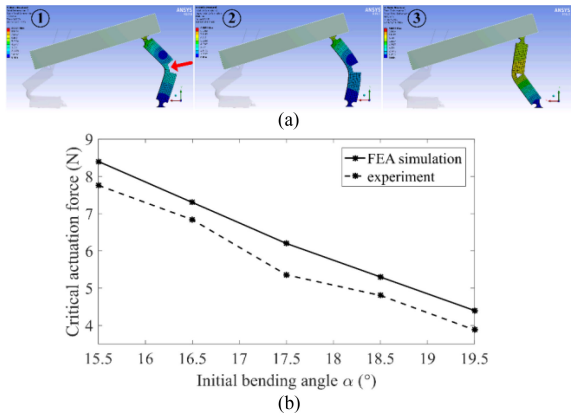

Fig. 9. (a) FEA simulation of the actuation process of the bistable structure; the actuation force is applied to the waist along the direction of the joint pin (indicated by the red arrow in ①). State ① is the starting point, which is the same as stage I in Fig. 5(b). State ② is the position at which the maximum actuation force $F_{P,\max}$ is generated. State ③ indicates that the bistable structure succeeded in switching between two stable states. (b) FEA results and experimental results of maximum actuation force [corresponding to $F_{P,\max}$ in Fig. 5(a)] with respect to the initial bending angle.

bistable states transition. In the simulations, the force applied to the waist was set to increase gradually (each position was an equilibrium position), and it was automatically subdivided between 0 and 12 N, with resolution ranges from 1% to 5% by the software (Fig. 9(a), state ①). When the bistable structure reached the critical position, it generated snap-through buckling (Fig. 9(a), state ②), and the force was removed. The critical maximum bistable actuation force was then obtained. We simulated the required maximum actuation force at different initial bending angles (15.5°, 16.5°, 17.5°, 18.5°, and 19.5°), and the results indicated a trend similar to that of the experimental results. The resultant forces in the experiment were obtained by measuring the forces acting on one SMA spring and considering the direction of the resultant force. The results showed that the maximum actuation force decreased as the initial bending angle increased, but the magnitude of the experimental results was smaller than that of the FEA results. This can attribute to the fact that the initial bending angle cannot be fully fixed by the constraints of the cables and the counter bistable structure during the bistable actuation process, which means that it decreased slightly, leading to a reduction in the actuation force.

IV. Case Study: Articulated Soft Robot System

A. Robot System

Based on the design and actuation of the BBAJ, we developed an articulated soft robot as presented in our previous work [33]. This robot consists of seven BBAJs, and each joint has a pair of bistable structures. The entire robot is driven by one servomotor through cables.

The hardware architecture of the robot system is depicted in Fig. 10. The robot arm is driven by a servomotor (Hitec 7980TH) through steel cables, and the bistable structures are connected to each corresponding joint through a pair of SMA springs (Kellogg's Research Labs). The SMA springs are further

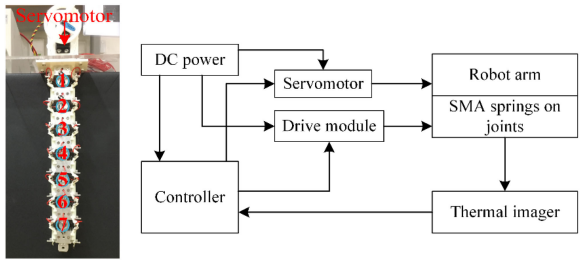

Fig. 10. Hardware architecture of the robot system.

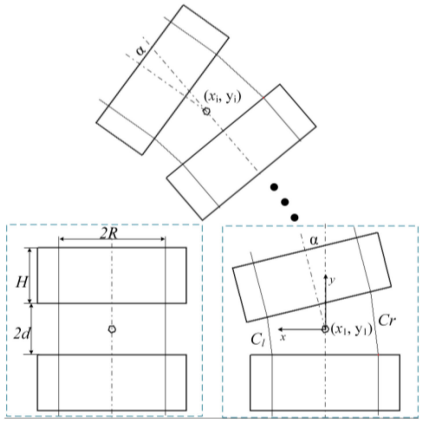

Fig. 11. Brief sketch of the joint's cable-driven motion.

connected to a dc power under 5 V (Topward 6306D dc power supply). The SMA springs are activated with the drive modules (BTN7971, a motor drive module that generates a large current) controlled using a microcontroller (Arduino mega2560). The SMA activation time is significant, and if the time for which it is activated is too long, its temperature increases excessively, leading to break the shape memory effect. Thus, we used a thermal imager (Optris PI) to visualize the temperature variation and provide feedback to control the activation of the SMA springs. Most of the components of the articulated soft robot arm were fabricated with 3-D printing and CNC machining, and the bistable structures were directly 3-D printed by Ultimaker S5 using soft materials (TPU 95A).

B. Kinematics and Workspace

The kinematics of the cable-driven articulated robot arm can be derived according to the geometric relationship. The bistable structures act as the elastic element of the robot arm, and they ensure that each joint bends nearly uniformly. A brief sketch of the joint is presented in Fig. 11. Changes in the lengths of the cables on both sides reflect the bending angle of the joint, and these changes are given as follows:

$$\begin{cases} \Delta C_l = -\left[2R\sin\frac{\alpha}{2} + 4d\sin^2\frac{\alpha}{4}\right] \\ \Delta C_r = 2R\sin\frac{\alpha}{2} - 4d\sin^2\frac{\alpha}{4} \end{cases} \tag{21}$$

where H is the length of the joint link, d *is* the distance between the rotation center and the joint, $2R$ is the distance between the parallel cables, α is the bending angle of the joint, and C_l and C_r are the lengths of the cables between the joints after bending.

TABLE I
PARAMETERS OF THE ROBOT

Parameters	Values
Joint limit bending angle α_{limit}	25°
Joint length $(H+2d)$	38 mm
Locking angle α_{lock}	15°
Cable distance $2R$	40 mm
Joint gap $2d$	18 mm
Neck length l_0	2 mm
Beam length l_1	9.5 mm
Waist length l_2	2 mm
Beam width w	3.6 mm

Because each joint is enabled LF and has three states, the robot has various configurations. We set 0, 1, and −1 to represent the free-bending, left-locking, and right-locking states, respectively. The robot can demostrate N^3 configurations by selectively locking the joints, where N is the number of joints. We defined a configuration matrix $M = [m_1\ m_2\ \ldots\ m_i]$, where $i = 1, 2, \ldots N$, and $m_i \in \{-1, 0, 1\}$, to derive the forward kinematics as follows:

$$\begin{aligned} x_{i+1}(t) &= x_i(t) + (H+2d)\cos\theta_i \\ &= x_i(t) + (H+2d)\cos \\ &\quad \times \left(\sum_{j=1}^{i} \left(m_j \alpha_{lock} + (1-|m_j|)\alpha_i(t) \right) \right) \\ y_{i+1}(t) &= y_i(t) + (H+2d)\sin\theta_i \\ &= y_i(t) + (H+2d)\sin \\ &\quad \times \left(\sum_{j=1}^{i} \left(m_j \alpha_{lock} + (1-|m_j|)\alpha_i(t) \right) \right) \end{aligned} \tag{22}$$

where θ_i is the bending angle of corresponding joint i in the reference coordinates.

From the configuration matrix, we can derive all the configurations of the robot. The robot fabricated in this article consists of seven joints, resulting in $3^7 = 2187$ different configurations. The idealization conditions in this kinematic model are that when one joint is locked, the counterforce of the opposing bistable structure and the LF prevent it from bending in both directions. However, in the deployment of the prototype, the locked joint can bend slightly in the unlocked direction. This is because the counterforce generated by the opposing bistable structure is insufficient to withstand the friction and moment generated by the cables. For each configuration, the tip point of the robot corresponds to the end effector. Therefore, the trajectory of the tip point represents the workspace of the end effector. For one-segment underactuated cable-driven robot arm without the LF, the workspace is a fixed trajectory. By contrast, the workspace of our robot with the joint LF is considerably larger, as shown in Fig. 12. The parameters of the robot are listed in Table I.

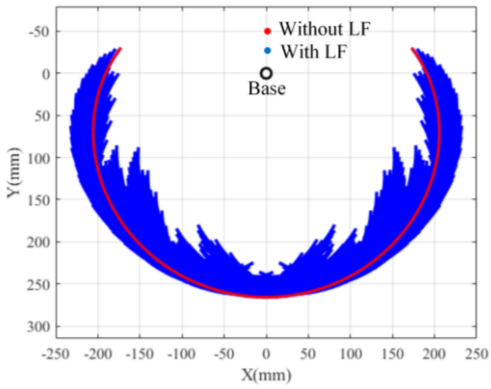

Fig. 12. Comparison of workspaces between a robot arm with an LF (blue area) and that without an LF (red curve). The resolution of this workspace is 500 × 500.

C. Stiffness Evaluation Metric

The stiffness change in our design is based on the state transition of the bistable structure in each joint, meaning that it is an ON–OFF change (not continuous). The magnitude of stiffness is determined by the selected materials, parameters of the bistable structure, and driving cables of the joint. However, when this type of articulated robot arm is used in the locked state, the cables normally do not bear load in the locking direction, and it is the bistable structure that supports the load of the arm without the cables. The high stiffness state of the joint is entirely determined by the materials selected and the design parameters of the bistable structure. Herein, we propose a stiffness evaluation metric for this featured approach.

We assume that the designed bending stiffness in the locking direction of each joint is k_b, which is determined by the materials and the design parameters of the bistable structure. The stiffness factors corresponding to the joint states in the locking direction are then separately set as high (f_h), medium (f_m), and low (f_l). For example, when a joint is in the left locking, the stiffness for driving the joint to bend toward the left is high, but the stiffness for driving the joint to bend toward the right is medium because of the counterforce of the opposing bistable structure in the joint. If the joint state is 0, then the stiffness on both sides is low.

The stiffness factors for bending toward the left are

$$f_{Li} = \begin{cases} f_h, & \text{if } m_i = 1 \\ f_m, & \text{if } m_i = -1 \\ f_l, & \text{if } m_i = 0 \end{cases} \tag{23}$$

The stiffness factors for bending toward the right are

$$f_{Ri} = \begin{cases} f_m, & \text{if } m_i = 1 \\ f_h, & \text{if } m_i = -1 \\ f_l, & \text{if } m_i = 0 \end{cases} \tag{24}$$

where $M = [m_1\ m_2\ \ldots\ m_i]$ is the configuration matrix from joint 1 to i. The stiffness factors can be obtained experimentally. Normally, we have $f_h \to 1^-$, $0 < f_m < 1$, and $0 < f_l < f_m$.

Based on the Cartesian stiffness matrix, the stiffness K_E seen at the end point of the manipulator can be expressed as [34]

$$K_E = J^{-T} K_\theta J^{-1} \tag{25}$$

where K_θ is the equivalent joint stiffness matrix and can be expressed as $K_\theta = \text{diag}([f_1 k_b, \ldots, f_i k_b, \ldots, f_N k_b])$; for bending toward the left, $f_i = f_{Li}$; and for bending toward the right, $f_i = f_{Ri}$. Based on (22), the Jacobian Matrix J can be expressed as Eq. (26) shown at the bottom of this page, where $\theta_i = \sum_{j=1}^{i}(m_j \alpha_{\text{lock}} + (1 - |m_j|)\alpha_i(t))$, as shown in (23). Here, J is a 7×7 matrix for seven joints after adding the identity matrix below.

Taken together, these rules constitute the stiffness evaluation metric for measuring the end stiffness of the articulated soft robot arm under different configuration matrices.

The joint LF determines the configurations and stiffness of the robot. The stiffness factors in this article were set to $f_h = 0.99, f_m = 0.4$, and $f_l = 0.1$ according to the test results, and the average bending stiffness of the single joint $k_b \approx 500$ N/m through tests. even though we have snipped the cable on the right side, it can bear a tip load (no energy is required at this moment) as well as maintain the shape and ensure safety owing to the joint stiffness. This property is promising for safely executing tasks that involve payload and manipulation with the end effector of the robot. Moreover, this robot can be easily extended in the 3-D space by using two orthogonal pairs of cables to drive the robot arm with a spherical joint, and more complex manipulators can be constructed by connecting multiple cable-driven segments in series with the BBAJs.

In this series-connected robot, for a single joint, the stiffness factor $0 < f_l < f_m < f_h$, and based on (24) and (25), when actuating series-connected articulated robot through cables, the most easily bending joints are in the free-bending state and are the opposite direction of the locking joint. As long as we actuate the robot not to approach the limit bending angle α_{lim} for the locked joints, we can avoid the automatic unlocking for the opposite locking direction.

V. Conclusion

In this article, we propose a new approach for the design of articulated soft robots with variable stiffness. The variable stiffness is achieved through the LF of each articulated joint. It is a mechanical stiffening method based on bistable structures and bistable actuation. Bistable structures can remain in stable states without requiring a continuous supply of energy. Thus, our robot has the advantage that when its joints are locked, they can retain their shape without actuation from the servomotor. Even when the cables snap, the joints can retain their shape when fully locked. One of the main contributions of this article is the identification of nature-based bistable actuation principles and the use of these principles to design a BBAJ. This joint has unique properties, such as three different states (free bending, left locking, and right locking), intrinsic compliance because of the bistable structures, variable stiffness through the LF, and locking at different angles with the use of mechanically preprogrammed bistable structures. We present a case study of an articulated soft robot using BBAJs. This robot exhibited unique advantages, even when driven by a single servomotor, including a large and variable workspace because of the thousands of different configurations, sustained shape without continuous power supply, and good load capacity because of the stiffness reinforcement provided by the LF.

This article is just the first step in utilizing structural bistabilities to develop robotic systems that feature a combination of softness and rigidity, and it offers a new vision of how to change the stiffness of soft robots. However, this article has a few limitations. For example, load capability can easily be improved by printing a composite bistable structure, which implies printing of the neck and waist by using soft materials and of the beams and ends by using rigid materials. Doing so would reduce the small deformations of the beams and improve stiffness under the LF. Another drawback of this design is that it requires the entire structure to fully bend to realize the LF at those angles. This might not be possible in some applications with limited available space. The friction of the BBAJ affects the uniform bending of the articulated soft robot arm, and a lubrication method, such as ring lubrication or grease lubrication, should be adopted to reduce it. The resilience of the material used to fabricate the bistable structures is crucial for achieving repeated deformation. The material used in this article was TPU 95A, which exhibited good resilience over hundreds of bending tests. However, for practical application, materials with higher resilience should be adopted. The trigger for the bistable structure in this article was supplied by the SMA. However, the SMA springs require tens of seconds to cool down at room temperature. This slow response speed makes them unsuitable for use in high-speed robotic systems. The use of SMA springs can be replaced with more speed-efficient actuation methods, such as the use of cable drives, magnetic force, and twisted-and-coiled actuators. The locking angle is mechanically preprogrammed according to the parameters of the bistable structures, and the structures cannot be locked at random angles. Although one can employ different bistable structures and multiple pairs of bistable structures on the joints to achieve locking at various angles, this solution is not very convenient or efficient for use in real-time tasks.

$$J = (H + 2d) \begin{bmatrix} (-s_1 - s_2 \cdots - s_i) & (c_1 - s_2 \cdots - s_i) & \cdots & (c_1 + c_2 \cdots - s_i) \\ (c_1 + c_2 \cdots + c_i) & (s_1 + c_2 \cdots + c_i) & & (s_1 + s_2 \cdots + c_i) \\ 0 & 0 & \cdots & 0 \\ & & 1 \quad \cdots & \\ \vdots & \vdots & \cdots & \vdots \\ 0 & 0 & & 1 \end{bmatrix} \tag{26}$$

In summary, we believe this article presents a new perspective for developing more versatile and functional articulated soft robots. The design principles and the bistable actuation properties demonstrated herein, including inherent compliance, variable stiffness, and large workspace, are favorable for robotic systems. In future works, we will improve this approach to the construction of variable-stiffness soft robots by optimizing the robot design and developing control algorithms for real applications.

References

[1] D. Rus and M. T. Tolley, "Design, fabrication and control of soft robots," *Nature,* vol. 521, pp. 467–475, 2015.

[2] M. Cianchetti, A. Licofonte, M. Follador, F. Rogai, and C. Laschi, "Bioinspired soft actuation system using shape memory alloys," *Actuators*, 2014, pp. 226–244, 2014.

[3] F. Gandhi and S. G. Kang, "Beams with controllable flexural stiffness," *Smart Mater. Struct.,* vol. 16, 2007, Art. no. 1179.

[4] F. Carpi, G. Frediani, C. Gerboni, J. Gemignani, and D. De Rossi, "Enabling variable-stiffness hand rehabilitation orthoses with dielectric elastomer transducers," *Med. Eng. Phys.,* vol. 36, pp. 205–211, 2014.

[5] A. Balasubramanian, M. Standish, and C. J. Bettinger, "Microfluidic thermally activated materials for rapid control of macroscopic compliance," *Adv. Funct. Mater.,* vol. 24, pp. 4860–4866, 2014.

[6] M. A. Mcevoy and N. Correll, "Thermoplastic variable stiffness composites with embedded, networked sensing, actuation, and control," *J. Composite Mater.,* vol. 49, pp. 1799–1808, 2014.

[7] N. G. Cheng, A. Gopinath, L. Wang, K. Iagnemma, and A. E. Hosoi, "Thermally tunable, self-healing composites for soft robotic applications," *Macromol. Mater. Eng.,* vol. 299, pp. 1279–1284, 2015.

[8] B. E. Schubert and D. Floreano, "Variable stiffness material based on rigid low-melting-point-alloy microstructures embedded in soft poly(dimethylsiloxane) (PDMS)," *RSC Adv.,* vol. 3, pp. 24671–24679, 2013.

[9] Y.-J. Kim, S. Cheng, S. Kim, and K. Iagnemma, "A stiffness-adjustable hyperredundant manipulator using a variable neutral-line mechanism for minimally invasive surgery," *IEEE Trans. Robot.,* vol. 30, no. 2, pp. 382–395, Apr. 2014.

[10] A. Stilli, H. A. Wurdemann, and K. Althoefer, "Shrinkable, stiffness-controllable soft manipulator based on a bio-inspired antagonistic actuation principle," in *Proc. IEEE/RSJ Int. Conf. Intell. Robots Syst.*, 2014, pp. 2476–2481.

[11] A. Shiva *et al.*, "Tendon-based stiffening for a pneumatically actuated soft manipulator," *IEEE Robot. Automat. Lett.,* vol. 1, no. 2, pp. 632–637, Jul. 2016.

[12] S. Li, D. M. Vogt, D. Rus, and R. J. Wood, "Fluid-driven origami-inspired artificial muscles," *Proc. Nat. Acad. Sci.*, vol. 114, pp. 13132–13137, 2017.

[13] M. A. Robertson and J. Paik, "New soft robots really suck: Vacuum-powered systems empower diverse capabilities," *Sci. Robot.,* vol. 2, 2017, Art. no. eaan6357.

[14] Y. Wei *et al.*, "A novel, variable stiffness robotic gripper based on integrated soft actuating and particle jamming," *Soft Robot.,* vol. 3, pp. 134–143, 2016.

[15] V. Wall, R. Deimel, and O. Brock, "Selective stiffening of soft actuators based on jamming," in *Proc. IEEE Int. Conf. Robot. Automat.*, 2015, pp. 252–257.

[16] T. Ranzani, G. Gerboni, M. Cianchetti, and A. Menciassi, "A bioinspired soft manipulator for minimally invasive surgery," *Bioinspiration Biomimetics,* vol. 10, 2015, Art. no. 035008.

[17] Y.-J. Kim, S. Cheng, S. Kim, and K. Iagnemma, "A novel layer jamming mechanism with tunable stiffness capability for minimally invasive surgery," *IEEE Trans. Robot.,* vol. 29, no. 4, pp. 1031–1042, Aug. 2013.

[18] A. Degani, H. Choset, A. Wolf, and M. A. Zenati, "Highly articulated robotic probe for minimally invasive surgery," in *Proc. IEEE Int. Conf. Robot. Automat.*, 2006, pp. 4167–4172.

[19] Z. Li, H. Ren, P. W. Y. Chiu, R. Du, and H. Yu, "A novel constrained wire-driven flexible mechanism and its kinematic analysis," *Mech. Mach. Theory,* vol. 95, pp. 59–75, 2016.

[20] L. L. C. Yuyu, L. Bo, W. Chao, W. Shuxin, and L. Dichen, "Design, fabrication and performance of a flexible minimally invasive surgery manipulator integrated with soft actuation and variable stiffness," *J. Mech. Eng.,* vol. 54, pp. 53–61, 2018.

[21] Y. Forterre, J. M. Skotheim, J. Dumais, and L. Mahadevan, "How the venus flytrap snaps," *Nature,* vol. 433, pp. 421–425, 2005.

[22] S. Patek, W. Korff, and R. Caldwell, "Biomechanics: Deadly strike mechanism of a mantis shrimp," *Nature,* vol. 428, pp. 819–820, 2004.

[23] J. R. Raney, N. Nadkarni, C. Daraio, D. M. Kochmann, J. A. Lewis, and K. Bertoldi, "Stable propagation of mechanical signals in soft media using stored elastic energy," *Proc. Nat. Acad. Sci.,* vol. 113, pp. 9722–9727, 2016.

[24] T. Chen, O. R. Bilal, K. Shea, and C. Daraio, "Harnessing bistability for directional propulsion of soft, untethered robots," *Proc. Nat. Acad. Sci.*, vol. 115, pp. 5698–5702, 2018.

[25] S.-W. Kim, J.-S. Koh, J.-G. Lee, J. Ryu, M. Cho, and K.-J. Cho, "Flytrap-inspired robot using structurally integrated actuation based on bistability and a developable surface," *Bioinspiration Biomimetics,* vol. 9, 2014, Art. no. 036004.

[26] S.-W. Kim, J.-S. Koh, M. Cho, and K.-J. Cho, "Towards a bio-mimetic flytrap robot based on a snap-through mechanism," in *Proc. 3rd IEEE RAS EMBS Int. Conf. Biomed. Robot. Biomechatron.*, 2010, pp. 534–539.

[27] V. Chalvet, Y. Haddab, and P. Lutz, "A microfabricated planar digital microrobot for precise positioning based on bistable modules," *IEEE Trans. Robot.,* vol. 29, no. 3, pp. 641–649, Jun. 2013.

[28] F. Mattioni, P. M. Weaver, and M. Friswell, "Multistable composite plates with piecewise variation of lay-up in the planform," *Int. J. Solids Struct.,* vol. 46, pp. 151–164, 2009.

[29] A. Pirrera, D. Avitabile, and P. Weaver, "On the thermally induced bistability of composite cylindrical shells for morphing structures," *Int. J. Solids Struct.,* vol. 49, pp. 685–700, 2012.

[30] D. N. Betts, H. A. Kim, C. R. Bowen, and D. Inman, "Optimal configurations of bistable piezo-composites for energy harvesting," *Appl. Phys. Lett.,* vol. 100, 2012, Art. no. 114104.

[31] W. Y. Lin and K. M. Hsiao, "Investigation of the friction effect at pin joints for the five-point double-toggle clamping mechanisms of injection molding machines," *Int. J. Mech. Sci.,* vol. 45, pp. 1913–1927, 2003.

[32] X.-F. Chen, J.-G. Hu, Y.-S. Xu, Z.-M. Xu, and H.-B. Wang, "Study on elastic dynamic model for the clamping mechanism of high-speed precision injection molding machine," *Shock Vib.,* vol. 2015, pp. 1–13, 2015.

[33] Z. Yong, D. Ruxu, W. Liao, and Y. Haoyong, "A novel articulated soft robot capable of variable stiffness through bistable structure," in *Proc. Int. Conf. Robot. Automat.*, pp. 2939–2945, 2020.

[34] G. Alici and B. Shirinzadeh, "Enhanced stiffness modeling, identification and characterization for robot manipulators," *IEEE Trans. Robot.,* vol. 21, no. 4, pp. 554–564, Aug. 2005.

Yong Zhong (Member, IEEE) received the B.Eng. degree in mechanical design, manufacturing, and automation from the Huazhong University of Science and Technology, Hubei, China, in 2011, the M.Eng. degree in control engineering from the University of Chinese Academy of Sciences, Beijing, China, in 2014, and the Ph.D. degree in mechanical and automation engineering from The Chinese University of Hong Kong, Shatin, Hong Kong, in 2017.

From 2017 to 2019, he was a Research Fellow with the Department of Biomedical Engineering, National University of Singapore, Singapore. He is currently an Assistant Professor with the Shien-Ming Wu School of Intelligent Engineering, South China University of Technology, Guangzhou, China. His research interests include mechanical design, kinematics, dynamics, and intelligent control, especially in the field of bioinspired robots, and soft robots.

Ruxu Du received the B.S. degree in electrical engineering and the M.S. degree in automatic control from the South China University of Technology, Guangzhou, China, in 1983, and the Ph.D. degree in mechanical engineering from the University of Michigan, Ann Arbor, MI, USA, in 1989.

From 1991 to 2001, he taught at the University of Windsor, Windsor, ON, Canada; at the University of Miami, Coral Gables, FL, USA; and at The Chinese University of Hong Kong (CUHK), Shatin, Hong Kong. Since 2002, he has been a Professor with the Department of Mechanical and Automation Engineering and the Director of the Institute of Precision Engineering, CUHK. He is currently a Professor with the Shien-Ming Wu School of Intelligent Engineering, South China University of Technology. His research interests include precision engineering, condition monitoring, fault diagnosis, manufacturing processes (metal forming, machining, plastic injection molding, etc.), and robotics.

Dr. Du became a Fellow of the American Society of Mechanical Engineers, in 2009, a Fellow of the Society of Manufacturing Engineers, and the Hong Kong Institute of Engineers, in 2012, and an Academician of the Canadian Academy of Engineering, in 2017.

Peng Guo received the B.Eng. degree in mechanical design, manufacturing, and automation, in 2011 from the School of Mechanics Science and Engineering, Huazhong University of Science and Technology, Wuhan, China, and the M.Eng. degree in mechanical engineering, in 2014, from the Changchun Institute of Optics Fine Mechanics and Physics, Chinese Academy of Science, Beijing, China, where he is currently working toward the Ph.D. degree.

Since 2014 March, he has been a Research Assistant with the Department of Photoelectric Detection, Changchun Institute of Optics Fine Mechanics and Physics, Chinese Academy of Science. His main research interests include support design and analysis of mirror in large-aperture optical telescope.

Haoyong Yu (Member, IEEE) received the Ph.D. degree in mechanical engineering from the Massachusetts Institute of Technology, Cambridge, MA, USA, in 2002.

He was a Principal Member of Technical Staff at the Defence Science Organisation National Laboratories, Singapore, until 2002. He is currently an Associate Professor with the Department of Biomedical Engineering and a Principal Investigator with the Singapore Institute of Neurotechnology, National University of Singapore, Singapore. His research interests include medical robotics, rehabilitation engineering, assistive technologies, system dynamics, and control.

Dr. Yu was the Recipient of the Outstanding Poster Award at the IEEE Life Sciences Grand Challenges Conference 2013. He has served on a number of IEEE conference organizing committees.